

Direct photonic production: towards high speed additive manufacturing of individualized goods

H. Schleifenbaum · A. Diatlov · C. Hinke ·
J. Bültmann · H. Voswinckel

Received: 15 February 2011 / Accepted: 16 May 2011
© German Academic Society for Production Engineering (WGP) 2011

Abstract World market competition currently boosts trends like mass customization and open innovation which result in a demand for highly individualized products at costs matching or beating those of mass production. This work focus on the resolution of the production related dilemma between scale and scope, e.g. either the low-cost production of high quantities or the high-end and thus cost-intensive low-volume production of individualized goods. One of the areas of greatest potential for the resolution of this dilemma are rapid manufacturing (RM) technologies due to their almost infinite geometrical variability and freedom of design without the need for part-specific tooling. Selective Laser Melting (SLM) is one of the RM technologies that additionally provides series identical mechanical properties without the need for downstream sintering processes, etc. However, the state-of-the-art process and cost efficiency is not yet suited for series production. In order to improve this efficiency and enable SLM to enter series production it is indispensable to

increase the build rate significantly by means of increased laser power and larger beam diameters. To exploit this potential, a new generation production machine including a kW laser and an optical multi-beam system is developed and experimental results and real life components are shown.

Keywords Selective laser melting (SLM) · Individualized series production · Machine design · Laser processing

1 Introduction

Today, industrial companies are challenged by a highly dynamic environment, which compels them to develop and manufacture products at a high level of flexibility and quality at low costs. The fast and global transfer of information and open markets are, besides the economic aspects, the main drivers of changing the global structure of manufacturing [1].

Considering industrial production in high-wage countries today, these trends can be cut down on two dilemmas that are closely related to each other (see Fig. 1) [2]. The first dilemma refers to the “value-oriented versus planning-oriented” production. The former approach (value orientation) focuses on value adding processes without the consideration of planning-, preparation-, handling- and transport processes whilst the latter focuses on extensive planning in order to optimize value-adding (i.e. modeling, simulation, information gathering, etc.).

The second dilemma is related to the “scale-scope” dimension. Either the production system is designed for high scale output without variances in the product design (critical masses, business and manufacturing process

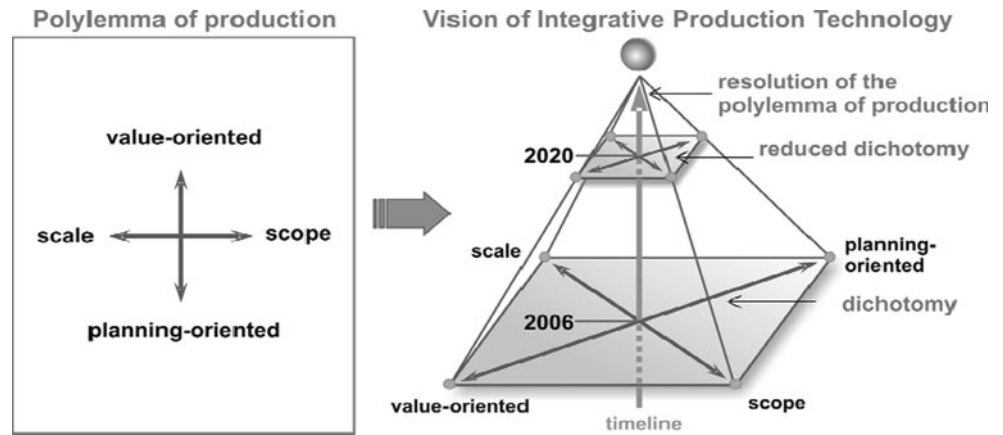
H. Schleifenbaum (✉)
Fraunhofer-Institute for Laser Technology (ILT),
Steinbachstraße 15, 52074 Aachen, Germany
e-mail: henrich.schleifenbaum@ilt.fraunhofer.de
URL: www.ilt.fraunhofer.de

A. Diatlov · C. Hinke
Chair for Laser Technology (LLT), RWTH Aachen,
Steinbachstraße 15, 52074 Aachen, Germany

J. Bültmann
Department of Ferrous Metallurgy (IEHK),
RWTH Aachen, Intzestr. 1, 52072 Aachen, Germany

H. Voswinckel
Institute of Metal Forming (IBF), RWTH Aachen,
Intzestr. 10, 52072 Aachen, Germany

Fig. 1 The polylemma of production



decomposition, mastered processes) or it is designed for individual products down to a production batch of a unique product, i.e. complex and highly integrated processes. The resolution of this production-related polylemma is the main target of the Cluster of Excellence “Integrative Production Technology for High Wage Countries” (see Fig. 1).

Especially the scale-scope dilemma is boosted by global trends like mass customization and open innovation which result in a highly fluctuating demand for individualized products at costs matching or beating those of mass production. One of the areas of greatest potential for the resolution of this dilemma are Additive Manufacturing (AM) technologies due to their almost infinite geometrical variability and freedom of design without the need for part-specific tooling. Selective Laser Melting (SLM) is one of the AM technologies for metallic parts that additionally provides series identical mechanical properties without the need of downstream sintering processes, etc. which predestines it for individualized manufacturing [3]. However, the state-of-the-art process and cost efficiency is not yet suited for series production and thus have to be improved.

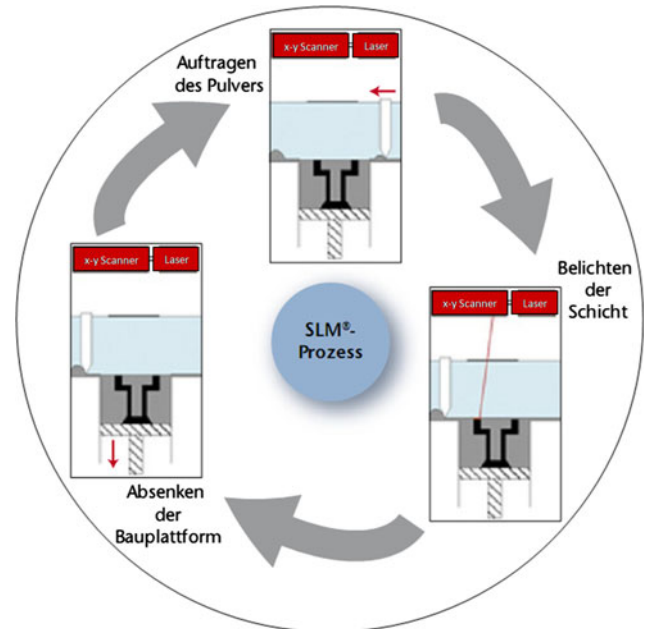


Fig. 2 Schematic representation of the SLM process

2 State of the art

2.1 Selective laser melting (SLM)

The ILT-developed SLM process is an Additive Manufacturing process that fabricates metallic components—layer by layer—directly from 3D-CAD data. This process enables the production of nearly unlimited complex geometries. The material used in the SLM process is a metallic or ceramic powder which is deposited as a thin layer (approx. 50 μm) on a substrate plate. The powder is selectively melted under an inert atmosphere by a laser beam according to the CAD model (see Fig. 2).

Subsequently, the substrate plate is lowered by one layer thickness and a new powder layer is deposited above. Again, this layer is selectively melted and metallurgically

bonded to the layer below. The scan direction is alternated after each layer in order to deter imperfections, which may occur during the melting process, from growing throughout several layers. Hence, the final component is built of many single layers. The use of standard metallic powders and the complete melting enables a density of approximately 100% which in turn assures mechanical properties that match or even beat those of conventionally manufactured parts.

In sum the SLM process enables a single component to combine the benefits of high geometrical freedom and functional integration with series suitable mechanical properties.

2.2 Build speed

Former research into Additive Manufacturing mostly focused on the qualification of new materials and their

industrial application. However, only little, if any research concerning SLM's process efficiency and therefore its build rate has been conducted yet. In order to come to a better understanding of the SLM process efficiency, the SLM process cycle time is divided into primary and auxiliary process time. The main process time only consists of the time that is needed to melt each single layer of a component whereas operations like substrate lowering and powder deposition are part of the auxiliary process time. With regard to this work the focus is on the primary process time because for a large volume that shall be additively manufactured this part of the total manufacturing time amounts to more than 80%. Large volumes can either consist of one large volume part or several low volume parts which are placed on a single substrate plate and manufactured simultaneously. Especially the latter one refers to the manufacturing of small or medium series production which shall be addressed with this work.

The main influencing variables of the primary process time are layer thickness (D_s), scanning velocity (v_{scan}) and scan line spacing (Δy_s). The process related build rate is calculated according to the following equation:

$$\dot{V}_{process} = D_s \cdot v_{scan} \cdot \Delta y_s \quad (1)$$

Scanning velocity and layer thickness are limited by the laser power available whilst scan line spacing is limited by

the focus diameter ($\Delta y_{s,max}$ typically equals approx. 0.7 times the beam diameter) [4]. Table 1 exhibits a comparison of the above mentioned process variables and the build rates published to date.

Yet, it was not stated in all papers mentioned in the table above if fully dense components were fabricated. Furthermore some authors investigated (two-component) sintering processes while others focused on melting processes but only investigated binding mechanisms within single layers and compared different materials. Hence, the depicted values of the parameters, especially the theoretical build rate (last column), assign a kind of limit value. By contrast, the last row depicts a set of parameters that originates from industrial applications and has been approved in own investigations on a series machine tool (Trumaform LF). The materials investigated are series-identical high alloyed steel (1.4404) and hot work tool steel (1.2343) respectively. The same materials were investigated in a benchmark conducted by "Laserinstitut Mittelsachsen" in close collaboration with "Fraunhofer-Allianz Prototyping" and "LBC GmbH". This investigation points out that the build rate of the same machine tool amounts 3–5 cm³/h, which is approx. 0.8–1.4 mm³/s [5]. Thus, the last-row value of the build rate is taken as benchmark for the following investigations.

Table 1 Summary of the influencing variables and build rates with regard to additive manufacturing of metallic powders

Source	Material	Laser source	Max. laser power* (W)	Beam diameter (scan line)** (mm)	Scanning velocity (mm/s)	Layer thickness (mm)	Theoretical build rate*** (mm ³ /s)
[4]	Stainless steel (X2CrNiMo17 12 3, X2CrNi24 12), tool steel (1.2343), nickel	Nd: YAG (cw)	105 W	0.2 (0.14)	<200	<0.1	<2.8
[9]	Tool steel (X38 CrMoV 5-1) titanium (TiAl6V4)	Nd: YAG (cw)	120 W	0.2	<250	<0.1	<3.5
[10]	Aluminium (AlSi25, AlSi10 Mg, etc.)	Nd: YAG (cw)	330 W	<0.4	<250	<0.1	<7
[11]	Stainless steel (1.4404), hot-work steel (1.2714), ni-base alloy (IN718)	CO ₂	200 W	0.1	50	0.05–0.1	0.5
[12, 13]	Stainless steel (X38 CrMoV 5-1 and X40 CrMoV 5-1)	No info	No info	≈0.4	No info	≈0.4	–
[14]	Titan (TiAl6V4)	No info	No info	<0.5	No info	0.13–0.38	–
[15]	Tool steel	Nd: YAG (pulsed)	550 (150)	0.9 (0.6)	<10	0.4	<2.4
[16]	WC–Co	Nd: YAG (cw)	60	0.8	30	0.2	2.5
[17]	Cu, Ni, Fe3P	CO ₂	60	0.3 (0.2)	<100	0.2	<4
[18, 2]	Stainless- and tool steel (1.4404 and 1.2343)	Nd: YAG (cw)	250	0.2 (0.15)	160	0.05	1.2

* If pulsed laser radiation was used, the 2nd number denotes the average laser power

** If no scan line spacing is given, the relation scan line spacing $0.7 \times$ beam diameter is used

*** According to formula 1

2.3 Increasing the build speed

The experiments conducted to date indicate that there is only limited scope to increase the build rate based on higher laser power and a corresponding increase in the scanning velocity at a constant beam diameter. Increasing the laser power while maintaining a constant beam diameter has the effect of increasing the intensity at the point of processing. This in turn leads to a higher evaporation rate resulting in a higher incidence of spattering which has a negative effect on the process as a whole. To avoid this, the beam diameter has to be enlarged. Schleifenbaum et al. [6] showed that satisfactory results can be achieved with regard to Selective Laser Melting of series-identical metallic powders by means of increased laser power (up to 500 W) and the correspondent adaption of the beam diameter to approximately 0.8 mm. Yet, the accuracy and detail resolution of additive manufactured parts are negatively influenced by larger melt pools which, as a general rule, grow with larger beam diameters and layer thicknesses [4].

In order to avoid this negative influence of larger melt pool geometries the so-called skin-core strategy has to be taken into consideration. According to this strategy the part to be built needs to be divided into an inner core and a skin which forms the outer contour of the part (see Fig. 3). Thus, different parameters for the outer skin and the inner

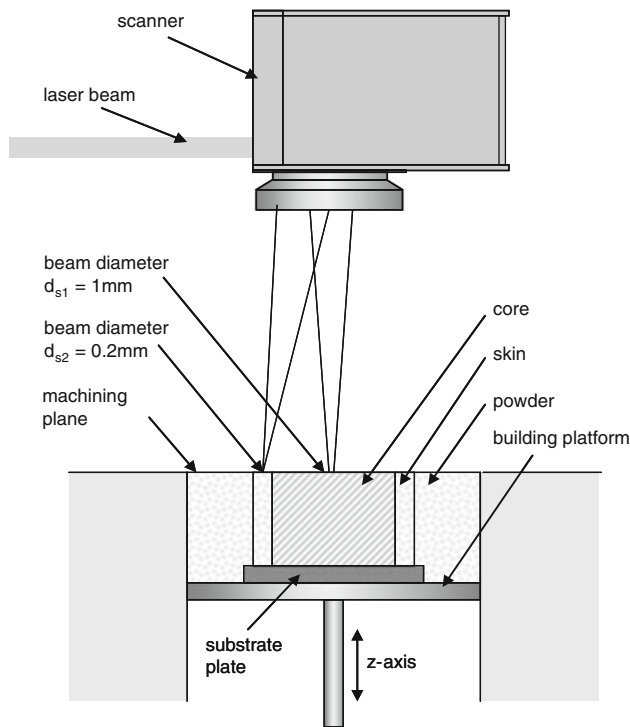


Fig. 3 Schematic representation of the skin-core concept

core of a component can be chosen. Both, skin and core must have a density of approximately 100% to assure the same mechanical properties as conventionally manufactured components. However, the core does not have strict limitations and/or requirements concerning accuracy and detail resolution. Hence, the core can be fast manufactured with a large beam diameter whilst the skin is manufactured with a small beam diameter in order to assure the part's accuracy and detail resolution. Figure 3 depicts the skin-core concept with different focus diameters.

3 Machine setup

As discussed above an increase of the build rate by means of increasing the beam diameter and layer thicknesses needs to be supported by higher laser power. Besides that, the new prototype plant must be equipped with a variable focus diameter in order to assure the accuracy of additively manufactured components.

To realize this new concept a Trumaform LF250 was completely rebuilt, both in terms of hardware and software. In order to increase the process related build rate beyond [6] the maximum laser power should be extended to more than 500 W. To date, the maximum laser power in commercially available SLM machines is limited to some 200 W [5]. Therefore, the integration of a new laser source (1 kW) is combined with the redesign of the optical system.

3.1 Optics

3.1.1 Power density distribution

Own investigations have shown that there is only limited scope to increase the build rate by means of high power lasers with a (single mode) Gaussian beam profile that causes an extremely high intensity in the beam centre. This again leads to an increased evaporation rate and thus in a higher incidence of spattering which may cause a process failure. Furthermore, the Gaussian beam profile shows less steep flanks which can limit the maximum possible scan line spacing since each powder grain needs a certain amount of energy to melt completely. Hence, the desired intensity distribution (i.e. uniformly or top hat shaped as it will be shown beneath) has to be taken into consideration when designing the new optical system. The amount of energy which is thermalized in a single powder grain is determined by the following equation.

$$E = A \cdot \iiint I(r, \varphi) \cdot r \, dr \, d\varphi \, dt \quad (2)$$

where »A« is the absorption coefficient, »I« the intensity distribution, »r« the radius and »φ« the plane angle.

Considering a rotationally symmetric Gaussian Intensity distribution in any distance »z« along the propagation direction the intensity distribution can be written as follows:

$$I(r, z) = I_0(z) \cdot e^{-\frac{2r^2}{w(z)^2}} \quad (3)$$

where » I_0 « is the maximum intensity and » w « is the full beam radius. This causes the powder grains that are “far” away from the beam centre, and thus from I_0 , to absorb less energy than the powder grains located in the beam centre. If the amount of energy is less than the thermal energy content of a powder grain, the grain is not (completely) molten. Thus, the solidified layer may show imperfections between single scan lines.

By contrast an ideally uniform intensity distribution is described by the following equation:

$$I(r, z) \approx I_0(z) \quad (4)$$

which is no longer dependant on the beam radius » r «. This can enable melting the powder grains nearly over the complete beam diameter. Hence, the scan line spacing can be enlarged in comparison to the possible scan line spacing of a Gaussian beam profile. This contributes to an increased build rate as shown by Eq. (1) while reducing the amount of spattering at the time due to the reduction of the maximum intensity in the beam centre.¹

In summary a uniform top-hat beam profile seems to be more suitable for additive manufacturing techniques especially in the case of large beam diameters and thus increased build rates. As a general rule, a top hat intensity distribution is boosted by the superposition of many transversal electromagnetic modes during the propagation through an optical multimode fiber. Hence, a fiber coupled high-power laser (1 kW) is opted for the integration into the SLM machine.

Yet, with this optical setup a top hat beam profile is not achievable when defocusing the laser beam, since the intensity distribution of non-fundamental modes change along the propagation direction. Thus, for the variation of the beam diameter, an optical system needs to be designed that enables the focused imaging of the optical fiber end at the machining plane.

3.1.2 Optical system layout

The product of the refractive index, the object and image height respectively and the angles of light rays within the

¹ Considering a constant beam diameter and constant laser power, the average intensity of all (round) beam profiles is equal. In the case of an ideally top hat shaped beam profile the average intensity corresponds to the maximum intensity I_0 whereas in the case of a Gaussian beam profile I_0 is much higher than the average intensity [see Eq. (3)].

paraxial object and image space is a conserved quantity of any optical system (see Eq. 6) [7]. In case of a small aperture angle of the optical system the sine of the angle can be approximated as follows:

$$\sin(\sigma') \approx \sigma' \quad (5)$$

Hence, the so-called Helmholtz-Lagrange invariant is written as follows:

$$n \cdot y \cdot \sigma = n' \cdot y' \cdot \sigma' \quad (6)$$

where » n « and » n' « are refractive indexes, » σ « and » σ' « are angles of light rays, and » y « and » y' « are object and image heights respectively. This relationship is always established between two zones on both sides of an optical surface (e.g. lens). Thus, an optical system that fulfils the Helmholtz-Lagrange invariant maps any point in the object space to a point in the image space (see Fig. 4).

The geometrical relationship between collimation and optical focusing (see Fig. 5) in combination with identical refractive indices before and after the optical system leads to Eq. (7).

$$d_{\text{focus}} = \frac{w_l \cdot f'}{w'_l \cdot f} \cdot d_{\text{fibre}} \quad (7)$$

where » w « and » w' « are beam radii on the focusing and collimating lens, » f « and » f' « are collimation- and focusing focal length, » d_{focus} « is the focus diameter and » d_{fibre} « the fiber diameter.

The variation of the beam diameters for the processing of skin and core is done by an automated fiber change (variation of d_{fibre}). The focus diameters realized with the setup depicted below (see Fig. 6) can be changed between 193 μm and 1,050 μm .

Since the optical fibers should not be exposed to mechanical forces like distortion, sharp bending, etc. the fiber switch is realized by a movable tilted mirror. This mirror can be moved into the course of the beam by means

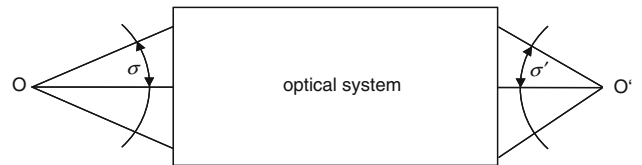


Fig. 4 Mapping of an arbitrary optical system

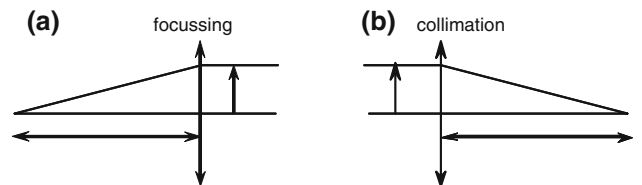
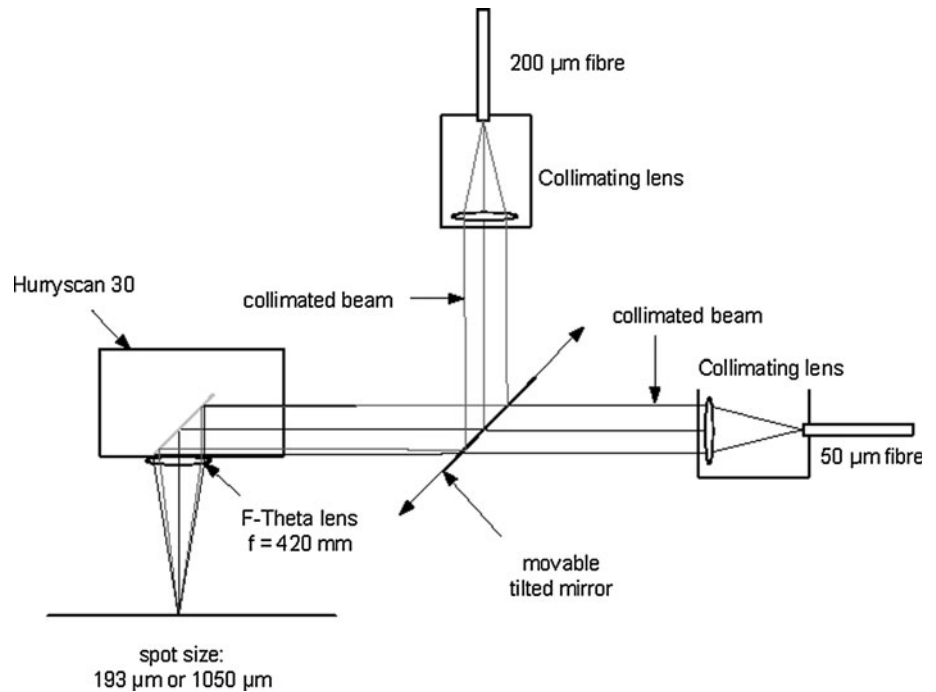


Fig. 5 Geometrical relationship for a focussing and b collimation

Fig. 6 Schematic representation of an automated fiber change



of a linear axis. The tilted mirror has to be moved parallel to the mirror plane in order to assure concentricity of the different beams in both end positions of the slide. By contrast the positional tolerance of the end positions themselves is noncritical for the concentricity. The laser beam is guided into a scanner system and focused to the machining plane by means of an f-theta lens. Additionally, this objective enables a sealed optical system, which prevents the deposition of dust particles on the scanner mirrors. The focus diameters in the depicted setup can be varied between 193 and 1,050 μm. Over and above these values the focus diameter at the machining plane can be varied between 100 μm and several millimeters by varying the collimating focal length, the fiber core diameters and by changing the focal length of the f-theta objective, see Eq. (7). Thus, a maximum flexibility of the setup can be assured.

Figure 7 depicts the new designed optical system that enables the automated change of optical fibers for the realization of different focus diameters at the machining plane. The principle shown is patent by Fraunhofer-ILT.

Since powder-polluted environment is not suitable for optical components, the beam switch is integrated into a solid housing. Thus, the optical system, i.e. scanner, beam switch, deflecting mirrors and collimation are completely sealed against powder and dust pollution. The complete optical setup realized is depicted in Fig. 8.

3.1.3 Fiber optics

As described above, a top hat beam profile is eligible for additive manufacturing techniques especially for a large

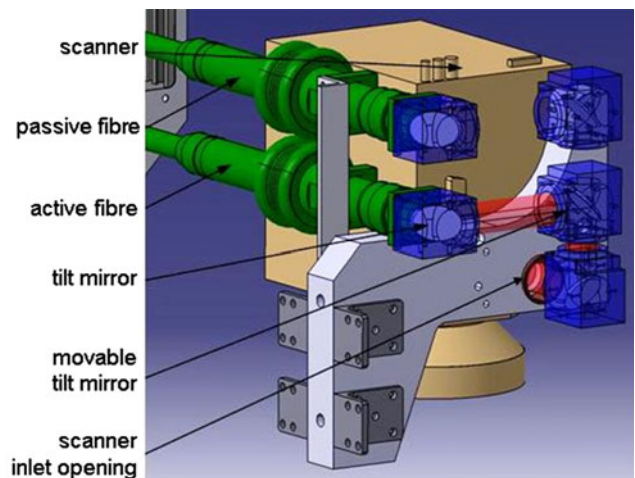


Fig. 7 3-D CAD volume model of the optical system for high power skin-core SLM applications, lower fiber active

scan line spacing which are inevitable for an increased build rate. Yet, a uniform intensity distribution requires the superposition of several modes over the running length of the fiber core. Furthermore not all rays that enter the fiber core are allowed to propagate (see Fig. 9) [7].

Considering a free wave the phase of the wave front C'A' concur in all single points. Hence, only waves whose phases concur in each point on the wave front AC can propagate through the waveguide [7]. Since this wave only consists of the incoming and the reflected wave, this constraint is fulfilled only if the phases of two rays differ in a multiple of 2π . Due to the incident-angle-dependant phase

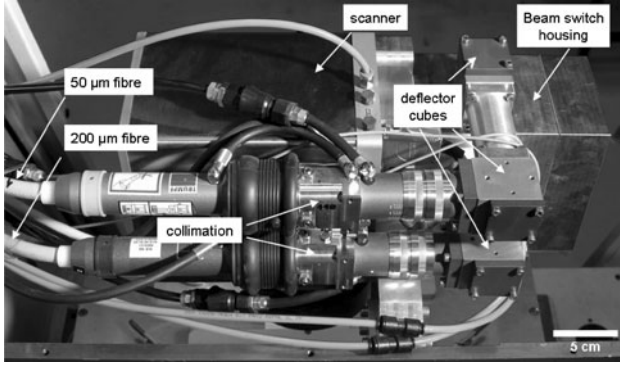


Fig. 8 Rear view of the optical system for high power skin-core SLM applications

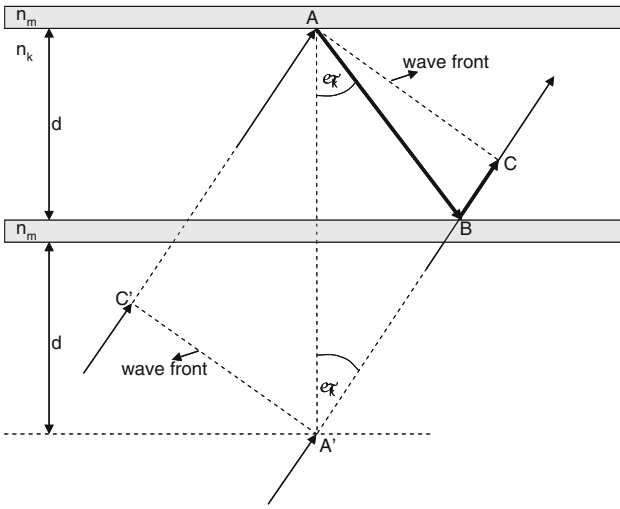


Fig. 9 Section of a planar wave guide. Rays are reflected at core-cladding interface. Allowed modes emerge in case of constructive interference

shift Ω the constraint for constructive interference becomes the following transcendent eigenvalue equation:

$$\frac{2 \cdot n_c d \cos(\varphi_{km})}{\lambda} = m + \frac{\Omega}{\pi} \quad (8)$$

where $\gg n_c \ll$ is the refractive index of the core, $\gg d \ll$ is the fiber core diameter, $\gg \lambda \ll$ is the wavelength and $\gg m \ll$ is the mode number. With regard to multi-mode fibers the second summand on the right side of the equation can be neglected since its maximum value is 1. Hence; the maximum number of modes m_{\max} occurs for the smallest possible angle—the critical angle for total reflection φ_g —which is calculated according to:

$$\varphi_g = \arcsin\left(\frac{n_c}{n_{cl}}\right) \quad (9)$$

where $\gg n_{cl} \ll$ is the refractive index of the fiber cladding. The numerical aperture NA is calculated according to:

$$NA = n_c \cdot \cos(\varphi_g) = \sqrt{n_c^2 - n_{cl}^2} \quad (10)$$

The combination of Eqs. (8–10) leads to the characteristic V-parameter for optical fibers:

$$V = \pi d \cdot \frac{\sqrt{n_c^2 - n_{cl}^2}}{\lambda} \quad (11)$$

The number of modes for cylindrical fibers, N , is finally calculated according to:

$$N = \frac{4}{\pi^2} V^2 \quad (12)$$

The probability to achieve a uniformly top hat shaped beam profile increases with the number of modes overlaying in an optical fiber. With regard to the optical setup used for the described prototype machine tool ($NA = 0.11$, $\lambda = 1030$ nm) the mode number of the 50 μm fiber is calculated to 114, whereas the mode number of the 200 μm fiber is calculated to 1,825. Although the absolute values do not indicate whether the resulting intensity profile is a top hat one or not, it becomes quite obvious that in the case of the smaller fiber core diameter (50 μm) the resulting intensity profile is more likely to be a Gaussian type than the intensity profile of the 200 μm fiber, whereas for the top hat intensity distribution it is vice versa.

In summary it can be estimated, that the intensity distribution for the manufacturing of the large volume core (where large build rates needs to be achieved) which is done with the 200 μm fiber, is likely to be a top hat one. In contrast, the outer skin is manufactured with the 50 μm fiber, whose intensity profile is more likely to be in between top hat and Gaussian shaped.

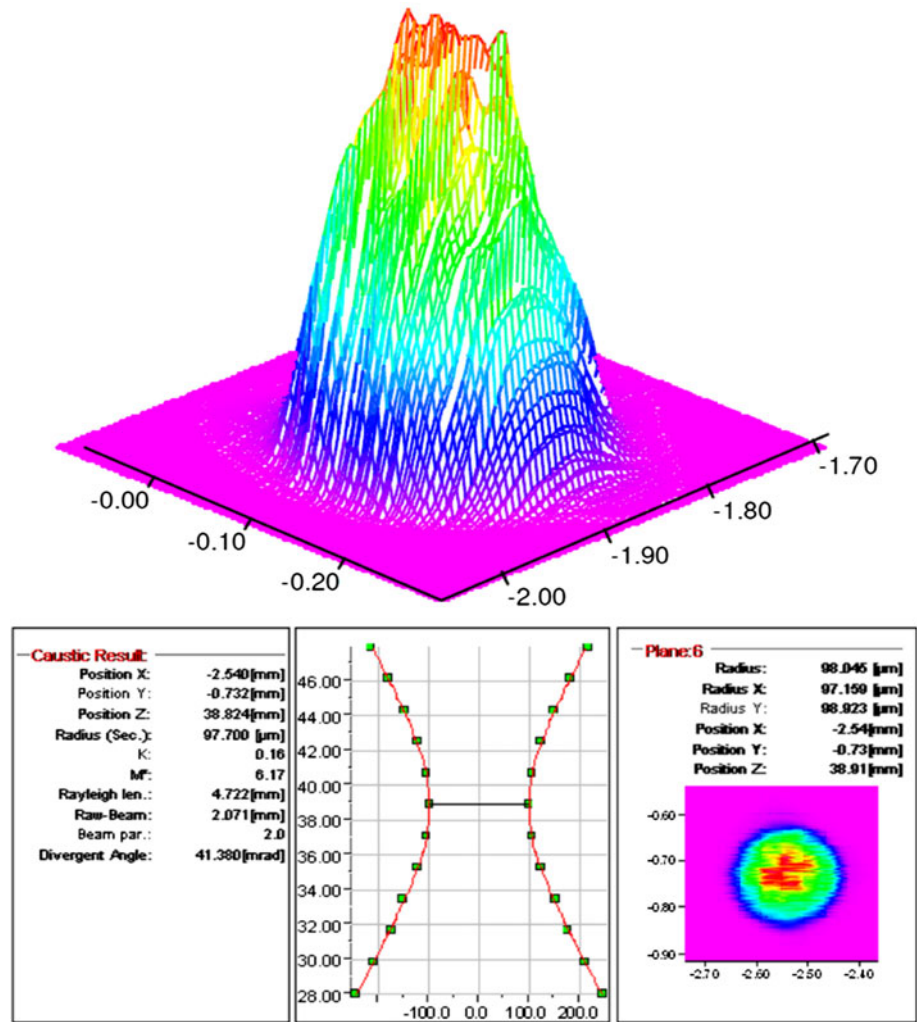
4 Findings

4.1 Beam caustic and power density distribution

As discussed above the shape of the beam profile largely depends on the number of modes exited throughout the optical fiber. Yet, the real shape also depends on other factors, especially the beam quality (determined by the resonator) and the geometrical setup at the incoupling end of the fiber. Since these specs are not accessible the caustic and the real beam shape have to be measured at the working plane to assure that the desired intensity distribution is achieved. Figure 10 exhibits the measurement results of the 50 μm fiber.

As it was estimated in chapter 3.1.1 the beam profile is somewhat in between Gaussian fundamental mode and top hat shaped. The flanks of the beam profile are steeper than those of a fundamental mode, whereas the top intensity is

Fig. 10 Caustic and intensity distribution (upper part: isometric view) 50 μm fibre



less complanate than a top hat beam profile. The focus radius measures 97.7 μm and M^2 is calculated to 6.17.

By contrast, the 200 μm fiber shows a M^2 of 30.6. As calculated in chapter 3.1.1 more modes can be excited throughout the 200 μm fiber which results in an homogenization of the intensity distribution and thus in a higher M^2 . Hence, in comparison to the beam profile of the 50 μm fiber, the beam profile at the working plane is more top hat shaped with steep flanks and a uniform intensity distribution (see Fig. 11).

The focus radius measures 532 μm which is slightly above the value calculated in the preceding chapter (525 μm).

4.2 Experimental results

The crucial factors for increasing the build rate are scan line spacing, scanning velocity and layer thickness. Whereas the former is limited by the beam diameter (approximately 0.7 times the spot diameter regarding 1.4404) [4] investigations by Schleifenbaum et al. [8] gave evidence that there is only limited scope in increasing the

build rate by means of increasing the scanning velocity. Hence, the main driver for increasing of the build rate can be found in the increase of the layer thickness. Therefore the scanning velocity was kept fix during the investigations discussed below.

In order to cope with the problem of incoupling the “right” amount of energy (space and time resolved) it is possible to vary the scan vector length. A short scan vector length causes the laser beam to alter its direction more often. I.e. the number of reversal points is increasing with a decreasing scan vector length. Within the area of those reversal points an increase of temperature can be observed since the energy source “rests” much longer on the reversal area than on a conventional hatch area. This superheating causes more powder particles to evaporate which result in the process instabilities described above. Therefore, decreasing the number of reversal points (i.e. increasing the scan vector length) decreases evaporation, spattering and process instabilities which is favourable for thinner layer thicknesses. Figure 12 exemplifies the density as a function of the layer thickness and different scan vector lengths.

Fig. 11 Caustic and intensity distribution (upper part: isometric view) 200 μm fibre

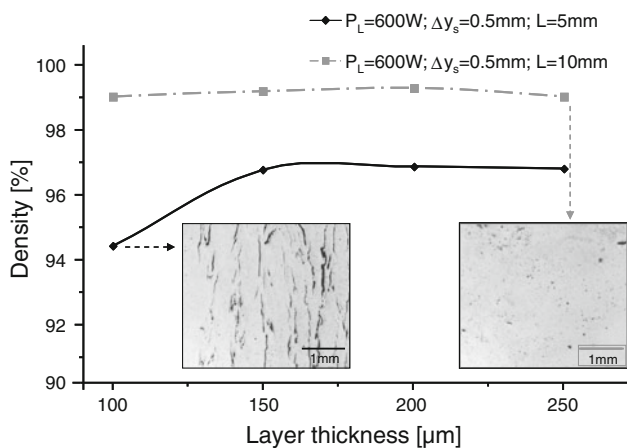
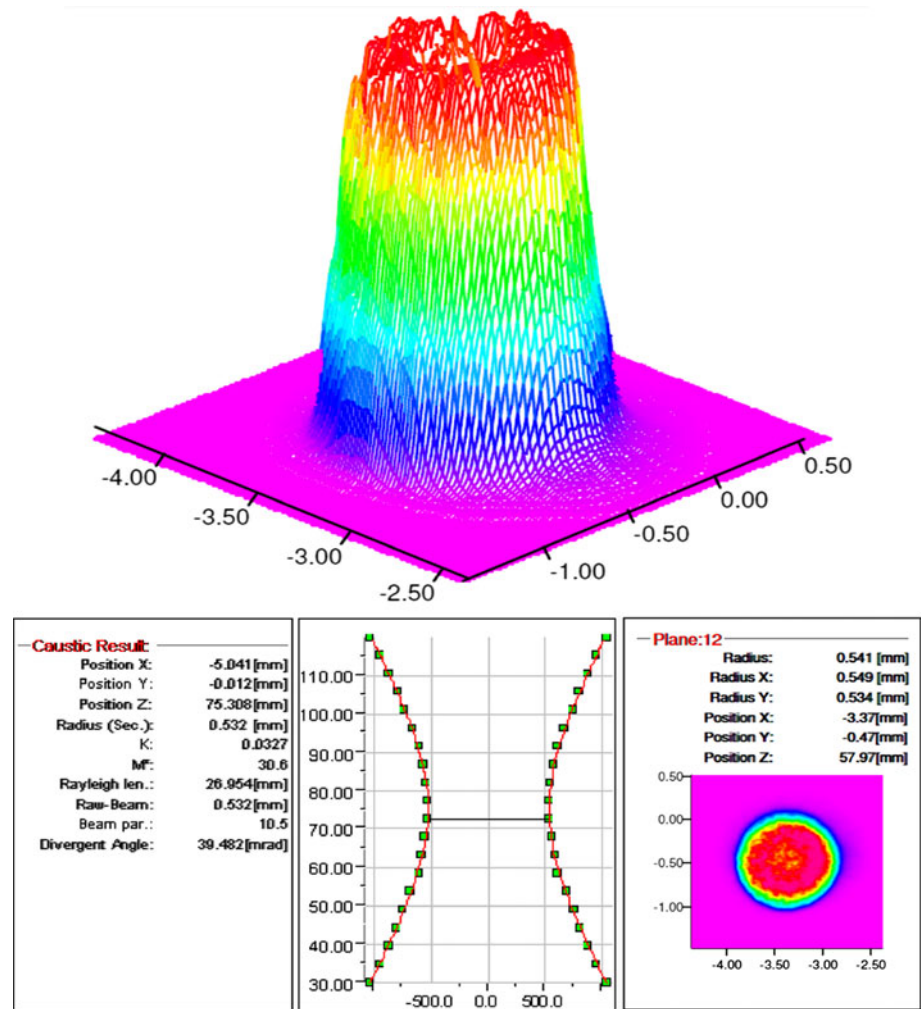


Fig. 12 Density versus layer thickness, comparison of scan vector length, beam diameter: 1.05 mm

Regarding the black graph (600 W, 5 mm scan vector length) the density increases from approximately 94% at 100 μm layer thickness to approximately 97% at 150 μm

due to higher amount of energy that is needed to melt the powder mass per scan line. Consequently superheating, evaporation and spattering decrease and the process becomes more stable. Yet, even with higher layer thicknesses, the amount of evaporation and process instabilities (especially in reversal points) is too big to assure the manufacture of dense components. The density of the manufactured specimen remains at approximately 97% up to 250 μm layer thickness.

Regarding the same process parameters, only varying the scan vector length from 5 mm to 10 mm, a significant advancement can be observed. Almost independent from the layer thickness (100–250 μm) the density of the specimen investigated remains unchanged. At a layer thickness of 100 μm the gap between 5 mm and 10 mm scan vector length amounts to approximately 5%. Due to the stabilization of the process with an increasing layer thickness this gap decreases down to approximately 2% at layer thicknesses between 150 μm and 250 μm . Hence a significant rise of the process stability and thus the part's density can be achieved by the implementation of longer scan vectors.

Fig. 13 Schematic representation of the skin core principle (*left*) and procedure of skin and core melting (*right*)

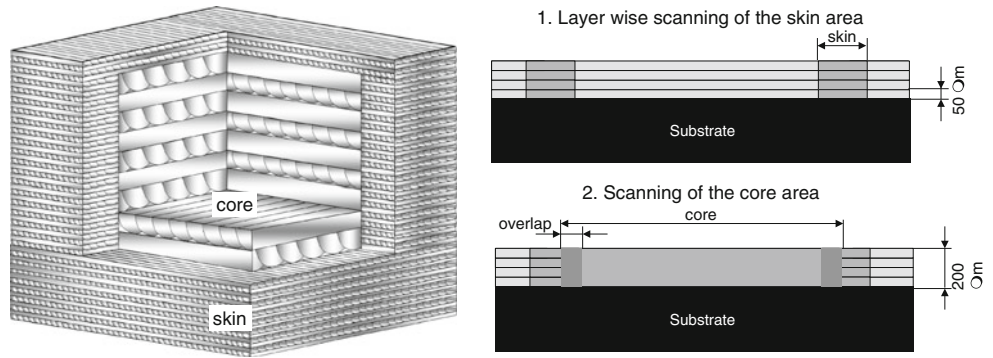
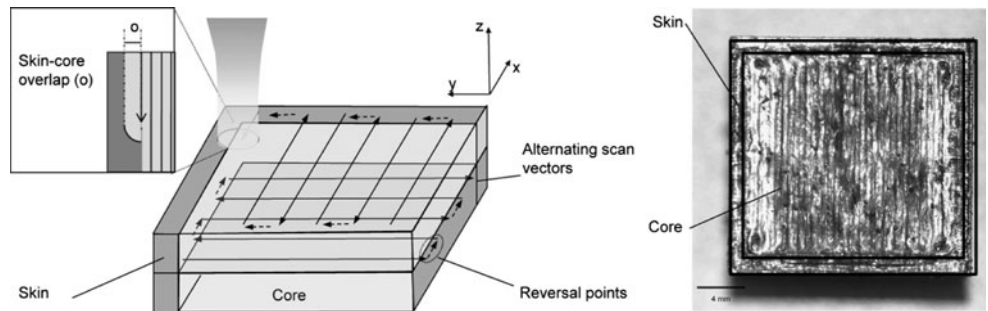


Fig. 14 Schematic representation of skin-core overlap (*left*), Skin-core specimen, top view (*right*)



Summing up, the experiments discussed above give evidence that an increase of the build rate by means of higher laser power and larger beam diameters needs to be backed by the implementation of longer scan vectors, especially if the layer thickness is comparable “thin”, i.e. less than 150 μm . The maximum build rate achieved within these experiments reaches up to 20 mm^3/s . Considering the current state of the art (see “State of the Art”) the build rate can be increased by more than 1500% while maintaining a density superior to 99%. Yet, accuracy, detail resolution and surface roughness are not tolerable for the manufacture of near net shape components. In order to avoid these disadvantages of an increased build rate by means of larger beam diameters and layer thicknesses, the outer part of the specimen can be manufactured by a smaller beam diameter (0.2 mm) at layer thicknesses inferior to 100 μm , e.g. 50 μm or 30 μm .

For the application of this skin-core strategy the specimen is subdivided into an inner and outer shell (see Fig. 13, left). The outer shell (skin), which is in this case 2 mm thick, is manufactured with the small beam diameter (0.2 mm) and a layer thickness of 50 μm . By contrast, the inner core is manufactured with a beam diameter of 1 mm. The core layer thickness can only be sized in multiples of the skin layer thickness, i.e. considering a skin layer thickness of 50 μm the core layer thickness can only be 100, 150, 200 μm , etc. (see Fig. 13, right).

A crucial factor for the metallurgical bonding is the overlap, i.e. the interface area that is scanned twice, of skin and core (see Fig. 14, left). This overlap has to be >0 mm.

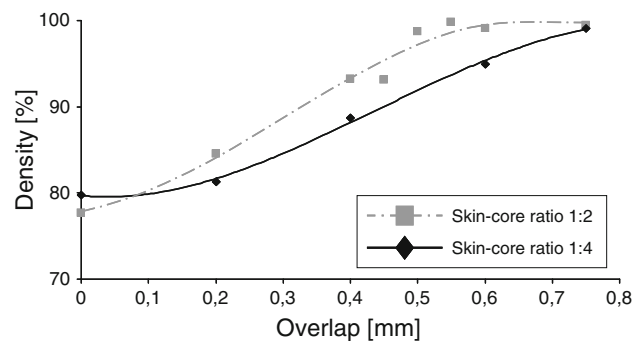


Fig. 15 Density of skin-core interface versus overlap, skin-core layer thickness ratios of 1:2 and 1:4

Figure 14 (right) exemplifies the manufacture of such a skin-core specimen. In this case, the core was manufactured with a spot size of 1 mm at a layer thickness of 200 μm , whereas the skin was manufactured with the small spot (0.2 mm) at a layer thickness of 50 μm .

In order to assure the metallurgical bonding of skin and core the overlap is varied depending on the skin-core layer thickness proportion (see Fig. 15).

For both investigated layer thickness ratios (1:2 and 1:4) the number and size of defects and thus the porosity is decreasing with an increasing overlap. Considering a skin-core layer thickness ratio of 1:2, i.e. in this case 50 μm skin layer thickness and 100 μm core layer thickness, a dense metallurgical bonding (density $>99\%$) can be assured with an overlap >0.5 mm. With regard to a skin-core layer

Fig. 16 Cross section of skin core specimen

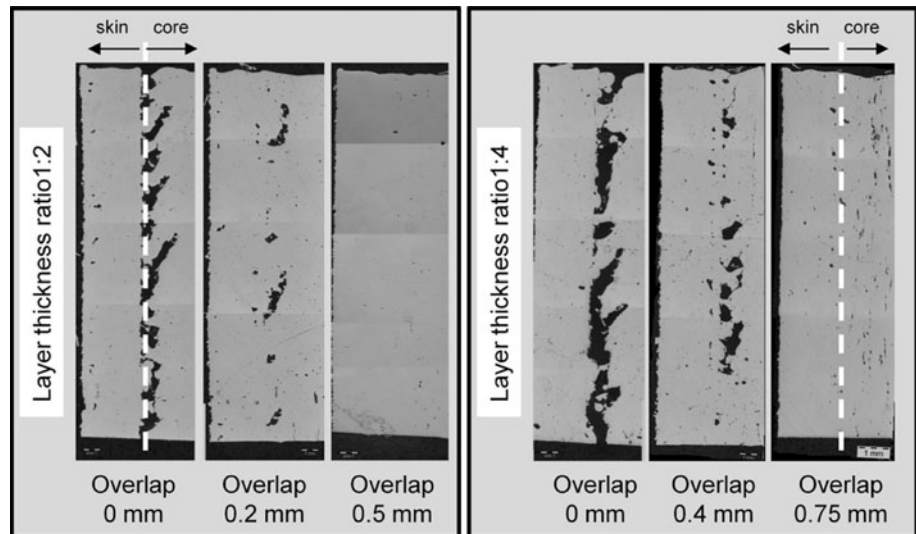
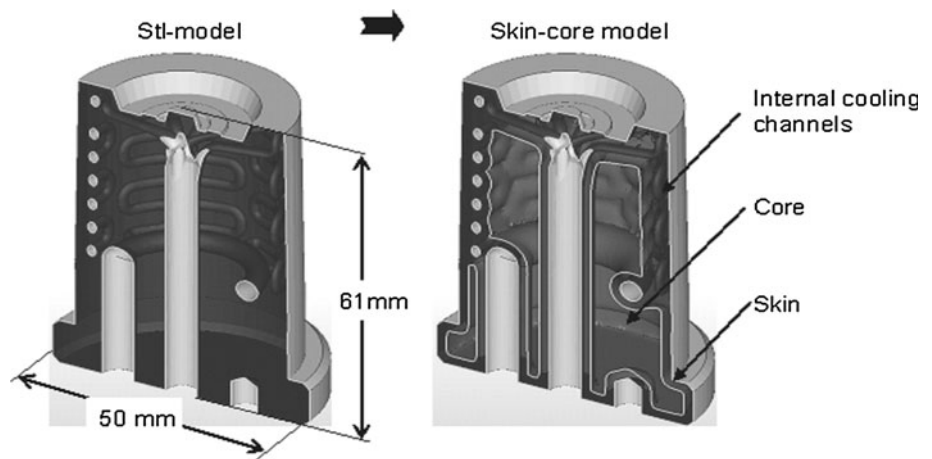


Fig. 17 3D-model of the complex tooling insert (left) and skin-core model (right)



thickness ratio of 1:4, i.e. in this case 50 μm skin layer thickness and 200 μm core layer thickness, a dense metallurgical bonding (density $>99\%$) can be assured with an overlap >0.75 mm. Figure 16 depicts the cross sections of such skin-core specimen with a layer thickness proportion of skin and core of 1:2 (left) 1:4 (right).

Though there is still some porosity detectable in the core part, the bonding of skin and core shows a density of approximately 100% for an overlap of 0.5 mm (layer thickness ratio 1:2) and 0.75 mm (layer thickness ratio 1:4) respectively. Hence, the manufacture of at least simple cubic skin core specimen with a layer thickness ratio of 1:4 (skin: 50 μm , core: 200 μm) is possible.

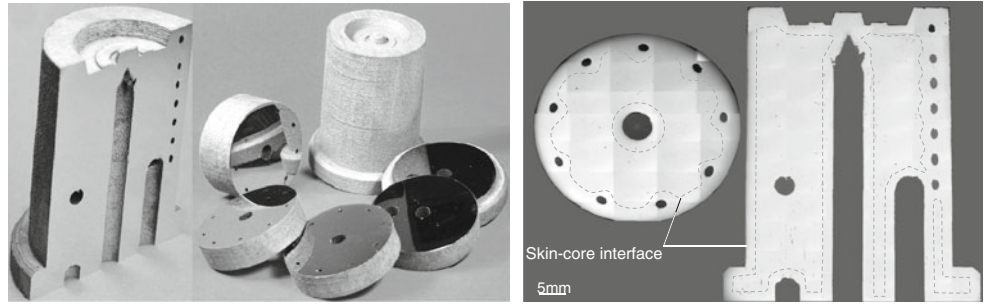
In order to demonstrate the potential of the skin-core strategy for the additive manufacture of complex real-life components with an increased build rate a demonstrator is built as shown in Fig. 17, left.

The part shown is a tooling insert for injection moulding. Due to the internal cooling channels the tool insert

cannot be built conventionally. Figure 17, right exemplifies the skin-core model of the tooling insert. In order to maximize the build rate while maintaining detail resolution and surface roughness the core layer thickness is chosen to 200 μm and the skin layer thickness to 50 μm . The resulting layer thickness ratio of 1:4 determinates the overlap to 0.75 mm (see chapter “Experimental Results—Skin-Core”). The additionally manufactured skin-core tool insert is shown in Fig. 18, left. In order to evaluate the density of skin, core and especially the bonding of skin and core, several cross sections are made (see Fig. 18, right).

The tooling insert shows a density of approximately 100%, i.e. the detectable porosity can be found in the range of conventionally SLM-manufactured specimen. The pores and sinkholes cannot be correlated to special area, neither skin and core nor skin-core interface. Hence, the manufacture of complex shaped skin-core parts with a layer thickness ratio of 1:4 (skin: 50 μm , core: 200 μm) is possible. The core build rate amounts to 16.8 mm^3/s , the skin

Fig. 18 Additively manufactured skin-core tool insert (left), cross sections (right)



build rate amounts to $3 \text{ mm}^3/\text{s}$. Hence, the overall process related build rate of the tooling insert amounts to $10.2 \text{ mm}^3/\text{s}$.

5 Summary and outlook

One of the key research targets in the Cluster of Excellence “Integrative Production Technology for High-Wage Countries” concerns solving this dilemma that opposes economies of scale and scope, e.g. either the low-cost production of high quantities or the high end and thus cost intensive low volume production of individualized goods. Selective Laser Melting represents one of the areas of greatest potential to reach this target. However, the state-of-the-art process and cost efficiency is not yet suited for series production.

In order to improve this efficiency and enable SLM to enter series production a new prototype machine tool was designed and built. For the first time a kW laser system was integrated into a SLM machine. In order to transform laser power into process efficiency, i.e. build rate, an optical system is designed that enables the additive manufacturing of components with an increased build rate. In order to maintain accuracy and detail resolution of additively manufactured components while increasing the build rate at the same time the optical system includes a new multi-beam concept that enables the processing with different focus diameters, layer thicknesses, etc. dependant on the part’s specifications (skin-core strategy). The experiments show that, with a spot diameter of 1 mm the core build rate of cubic geometries can be increased by more than 1,000% regarding the present state of the art. However, accuracy, detail resolution and surface roughness are not tolerable for the manufacture of near net shape components. Thus, the skin-core concept is firstly applied to cubic specimen and consequently to real-life parts, in this case a complex tooling insert with internal cooling channels. With regard to a layer thickness ratio of 1:4 the density of all areas of the part—skin, core and skin-core interface—reach approximately 100%. The process combined related build rate of the tooling insert amounts to $10.2 \text{ mm}^3/\text{s}$ which

represents a more than 8-fold increase with regard to the current state of the art.

Consequently, future research has to focus on developing a process conduct for even higher build rates as well in the core- as in the skin area. Furthermore it needs to be investigated if complex parts can be built with a layer thickness ratios $<1:4$. This will enable at least small lot series fabrication at costs matching or beating those of mass production, while retaining the ability to satisfy market demand for individualized products at the same time and finally help to SLM to break into new markets.

Acknowledgments The authors would like to thank the German Research Foundation DFG for the support of the depicted research within the Cluster of Excellence “Integrative Production Technology for High-Wage Countries”.

References

1. Schuh G, Monostori L, Csaji BC, Döring S (2008) Complexity-based modelling of reconfigurable collaborations in production industry. *Ann CIRP* 57(1):445–450
2. Schuh G, Klocke F, Brecher C, Schmitt R (2007) Excellence in production. *Apprimus*, Aachen
3. Schleifenbaum H, Meiners W, Wissenbach K, Hinke C (2010) Individualized production by means of high power selective laser melting. *CIRP J Manufact Sci Technol* 2:161–169
4. Meiners W (1999) Direktes Selektives Lasersintern einkomponentiger metallischer Werkstoffe. Dissertation, RWTH Aachen
5. Nische mit hohem Trendfaktor NN (2005) In: *Werkzeug und Formenbau*, pp 36–38
6. Kruth J-P et al (2005) Benchmarking of different SLS/SLM processes as rapid manufacturing techniques. In: *International conference polymers and moulds innovations (PMI)*, Gent, Belgium
7. Pedrotti F, Pedrotti L, Bausch W, Schmidt H (2002) *Optik für Ingenieure*. Springer, Heidelberg
8. Schleifenbaum H, Meiners W, Wissenbach K (2008) Towards Rapid Manufacturing for series production: an ongoing process report on increasing the build rate of Selective laser melting (SLM). In: *International conference on rapid prototyping and rapid tooling and rapid manufacturing*, Berlin, Germany
9. Over C (2003) Generative Fertigung von Bauteilen aus Werkzeugstahl X38CrMoV5-1 und Titan TiAL6V4 mit “Selective Laser Melting”. Dissertation, RWTH Aachen
10. Zhang D (2004) Entwicklung des selective laser melting (SLM) für Aluminiumwerkstoffe. Dissertation, RWTH Aachen

-
11. Wagner C (2003) Untersuchungen zum Selektiven Lasersintern von Metallen. Dissertation, RWTH Aachen
 12. Petersheim J (1997) Technologien zur direkten Herstellung funktioneller metallischer Prototypen. VDI Fachtagung "Rapid Prototyping—Neue Wege zur schnellen Fertigung von Modellen und Prototypen"
 13. Petersheim J (1997) Selektives Laserschweißen—Ein neuartiges Verfahren zur schnellen Fertigung mechanischer Bauteile. *Elektrowärme Int* 55(B3):B80–B85
 14. Kobyrn PA, Semiatin SL (2001) Mechanical properties of laser-deposited Ti-6Al-4 V solid freeform fabrication symposium, Austin, USA
 15. Su W-N et al (2003) Investigation of fully dense laser sintering of tool steel powder using a pulsed Nd: YAG (neodymium-doped yttrium aluminium garnet) laser. In: *Proceedings of the institution of mechanical engineers*, vol 217, Part C. *J Mech Eng Sci*, pp 127–138
 16. Wang XC et al (2002) Direct selective laser sintering of hard metal powders: experimental study and simulation. *Int J Adv Manufact Technol* 42:351–357
 17. Kruth J-P et al (2005) Statistical analysis of experimental parameters in selective laser sintering. *Adv Eng Mat* 7(8): 750–755
 18. Meiners W (2007) Personal communication, Fraunhofer-ILT